

An ROV-based sensor system for maritime pollution control

Frank Gereit^{*}, Peter Hauptmann⁺, Gerhard Matz[†],
Volker Mellert[‡] and Rainer Reuter[‡]

^{*}RST Rostock Raumfahrt und Umweltschutz GmbH, D-18119 Rostock-Warnemünde

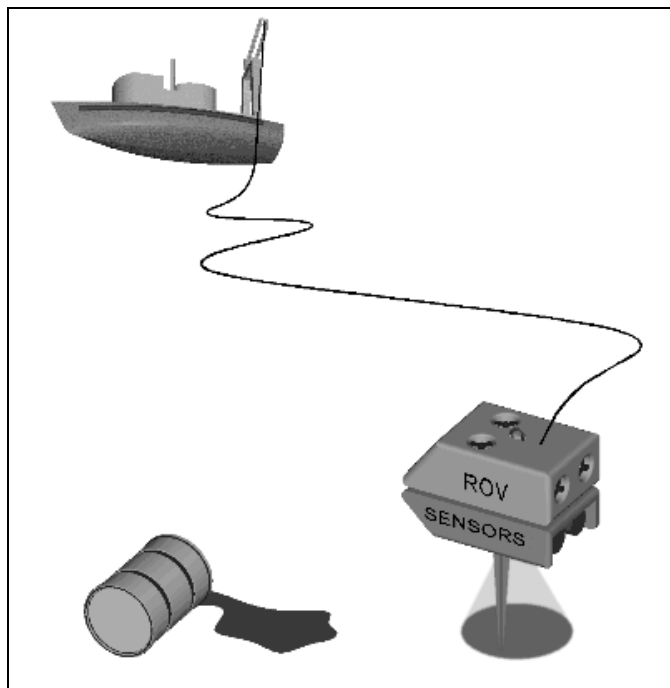
⁺Universität Magdeburg, D-39016 Magdeburg

[†]Technische Universität Hamburg-Harburg, D-21079 Hamburg

[‡]Carl von Ossietzky Universität Oldenburg, Fachbereich Physik, D-26111 Oldenburg

1 INTRODUCTION

The detection of chemical pollutants at sea is a difficult task when compared with oil spill survey. Mineral oil is mostly floating on the sea surface and therefore easily detectable aboard a ship or with remote sensing. An identification of oil-like chemicals on the sea surface with optical methods is often hampered because of their transparency which is mostly higher than that of oil. Other types of chemicals transported at sea mix with water and are rapidly dispersed, or sink to the seafloor because of their higher density and low solubility. Cargo can get lost from ships due to accidents or unfavourable weather, with the risk of harmful substances seeping out at the bottom from leaks in damaged containers. This situation makes a localization of chemicals discharged at sea, and hence pollution combating and clean-up operations very difficult or even impossible.^{1,2}



Principle of operation of the remotely operated vehicle (ROV) and its sensor payload.

To make available the technical means for counteracting such events, it has been decided by the German Ministry for Research and Technology to develop a remotely operated vehicle (ROV) equipped with instruments for localizing and analyzing chemical pollutants in the water column and on the seafloor. It is intended to operate this system on board the multi purpose vessel „Neuwerk“ of the Ministry of Transport in the German Bight. Because of the vast number of possible scenarios, the system consists of several sensors using various chemical and physical principles. In addition to basic sensors such as underwater video cameras and probes for measuring seawater temperature, conductivity and pH, the payload includes several newly developed instruments:

- a lidar for the inspection of the seafloor, which combines an ultrafast camera for an contrast-enhanced imagery of objects with a time-resolved fluorometer for substance classification,
- an acoustic sensor for measuring the acoustic impedance of the seafloor/water column interface which depends sensitively on the presence of surface films such as non-mixing chemicals spread on the ground,

- a membrane induction/gas chromatograph/mass spectrometer, and a
- quartz microbalance sensor array, both suitable for sensitive measurements of substances mixing with water, and sinkers on the seafloor that produce plumes with low concentrations of chemicals.

2 REMOTE SENSING INSTRUMENTS

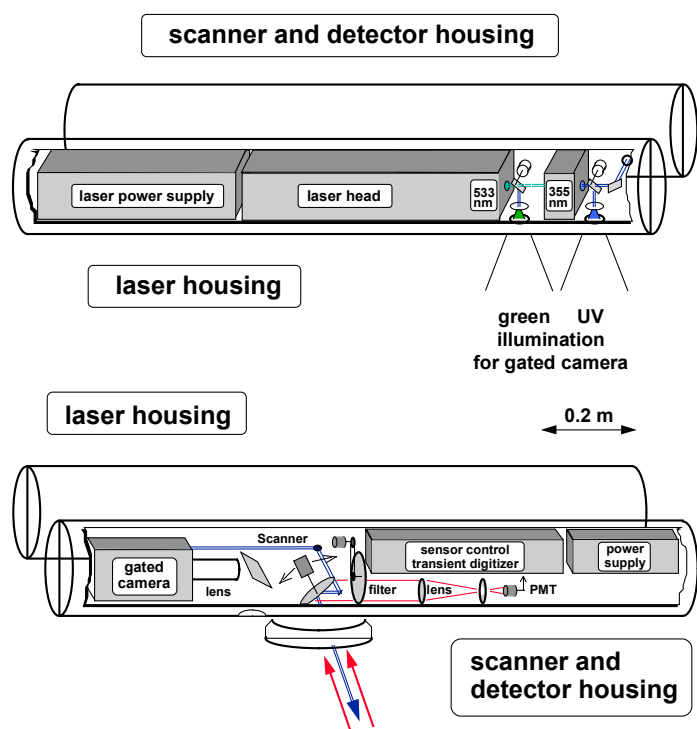
2.1 The lidar

The submarine lidar is a combination of a fluorescence lidar and a range gating video camera, with a Nd:YAG laser as the light source. The range gating video camera takes contrast enhanced images from the seafloor in turbid waters. Therefore it is used to search for and to inspect containers on the ground. The fluorescence lidar is used to detect chemicals which are often invisible on video images. The analysis of fluorescence spectra allows to classify substances.

The lidar is a remote sensing instrument. Data from the seafloor are remotely recorded, without any damage to the ecosystem. An altitude of a few metres above ground prevents sediment from rising and reducing visibility. This avoids also a contamination of the ROV in the presence of toxic substances on the seafloor.

2.1.1 Technical layout

The housing of the lidar is made of two titanium cylinders for the Nd:YAG laser, and the gated camera and lidar receiver unit, respectively. Electromagnetic interference produced by the pulse laser is very critical since it might degrade the quality of small lidar signals. The concept of using separate cylinders for the laser and the detector assembly, which is most sensitive to interference, reduces this disturbing noise.



Schematic drawing of the underwater lidar, with the Nd:YAG laser installed in the laser housing (above) and the scanner, gateable camera and spectrograph in the receiver unit (below). Length and diameter of the titanium cylinders are 1.2 and 0.2 m, respectively.

The laser has 160 mJ pulse energy at 532 nm and 60 mJ at 355 nm, and 4 ns pulse duration. Three illumination modes are realized by the use of tilting mirrors: UV emission as the light source of the fluorescence lidar, and the beam expanded green emission for illumination of the seafloor when taking video images. With the use of a blocking filter in front of the camera lens, the beam expanded UV

emission can be used for recording fluorescence images. The divergence of the expanded beams is adapted to the 1 rad camera field of view.

Video images are taken with a gateable intensified CCD camera with 520 x 736 pixel resolution and 8 bit dynamic range. Its minimum gate-on time is 5 ns. The maximum image repetition frequency is 20 Hz.

Fluorescence can be measured from small spots on the ground at positions that can be selected with an optical scanner. The receiver consists of a telescope with 50 mm free aperture, optical filters, a fast photomultiplier and a PC card transient recorder with 500 Mhz sampling rate and 8 bit resolution. Wavelength selection is done with a filter wheel, equipped with a semi-circular variable interference filter for the 400 to 700 nm range and four interference filters for the 355 to 400 nm range. An 80 dB high speed logarithmic amplifier compresses the photomultiplier signals before digitization to enhance the dynamic range.

A miniaturized PC selects the illumination modes, operates the transient recorder and organizes the data transfer between the instrument and the deck unit on board the ship.

2.1.2 Range gating video

An underwater image can be regarded as a linear superposition of three components, that are (i) backscattered light from the water column between the instrument and the target, (ii) reflected light from the target, and (iii) light reflected by the target and forward scattered in the water.³

The first component does not include any information about the target. It can be efficiently suppressed with range gated imaging: due to the laser pulses with a pulse length of 5 ns only, backscattered light from the water column reaches the camera prior to the other two components. It is faded out when setting the gate-on time of the camera to this time lapse, which results in a record of light reflected by the object only. This generally results in a contrast enhanced video image.

The second component consists of the light following a direct path of rays from the target to the detector, thus forming a sharp image of the target. Its quality follows from the optical transfer function of the camera, while image intensity and signal-to-noise ratio depend on the attenuation of light in the water.

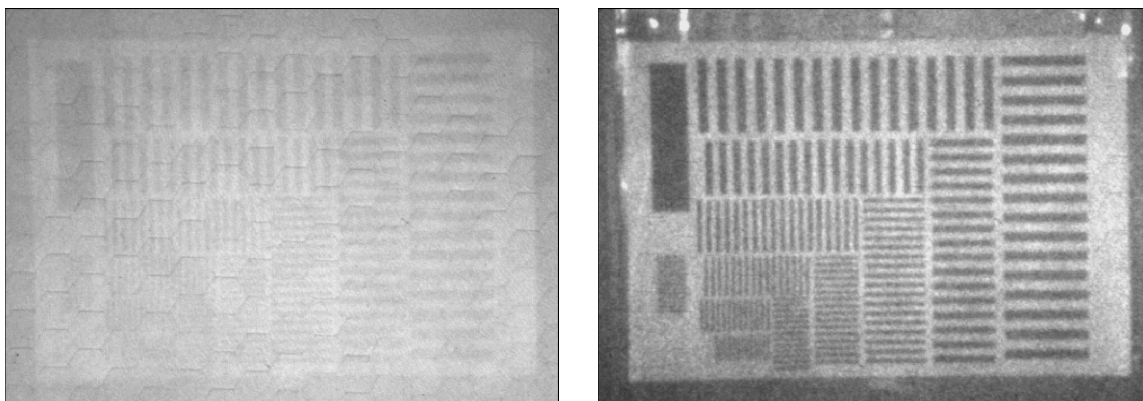


Image from a test target in a water tank at 10 m distance from the camera, with gate time = ∞ (left) and 5 ns (right), illuminated by a laser pulse with 532 nm wavelength and 5 ns pulse length. Attenuation of the water corresponds to coastal conditions.⁶

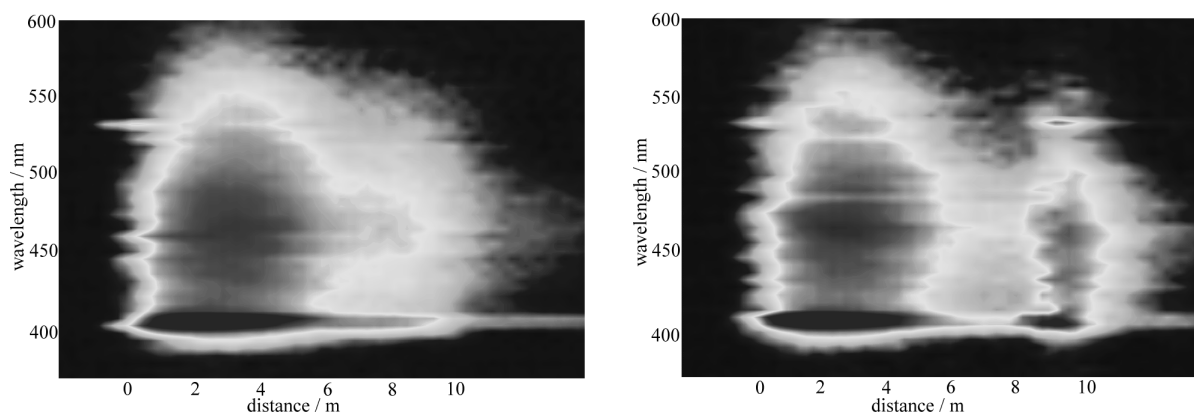
The third component, that is light reflected by the target and then forward scattered at small angles between target and camera, reaches the detector at virtually the same time as the second component. Hence, a separation from direct target reflections is not possible by their time of flight. The result is a blurred image which corresponds to the convolution of the original im-

age and the point spread function⁴ describing the optical characteristics of the water. The un-blurred image can be reconstructed if the point spread function is known.⁵

2.1.3 Fluorescence

Following the detection of a target with the video camera, a fluorometric inspection can be done with lidar. For this, the 3rd harmonic Nd:YAG laser pulse (355 nm, 4 ns, 60 mJ) is used with its original 0.5 mrad beam divergence. The emission of the target and the water column is recorded with 500 MHz sampling rate at wavelengths which can be set between 380 and 700 nm. Laser pulse length and receiver sampling rate lead to a maximum depth resolution of about 0.2 metres. With the scanner, records can be gathered from every point in the water column and target on the seafloor within the instrumental field of view.

The analysis of time-resolved signals at specific emission wavelengths allows to detect, locate and classify fluorophores.⁶ Non-fluorescent substances in the water influence the penetration depth of the lidar due to absorption losses. This effect can be utilized to indirectly estimate their concentration, which includes non-fluorescent chemicals dispersed in the water column.⁷



Lidar signals from a homogeneous water column (left) and the same water but with a fluorescent chemical at 9 m distance.⁷ Abscissa: distance derived from the time lapse between laser firing and signal return, ordinate: emission wavelength. The sensitivity function of the telescope and the attenuation of the laser beam determine the intensity distribution over distance. Clear water signals originate from water Raman scattering at 400 nm and fluorescence of dissolved organic matter with a maximum at 450 nm. In addition to this, an intense fluorescence is found in the presence of the chemical which allows its detection.

2.2 The acoustic impedance sensor

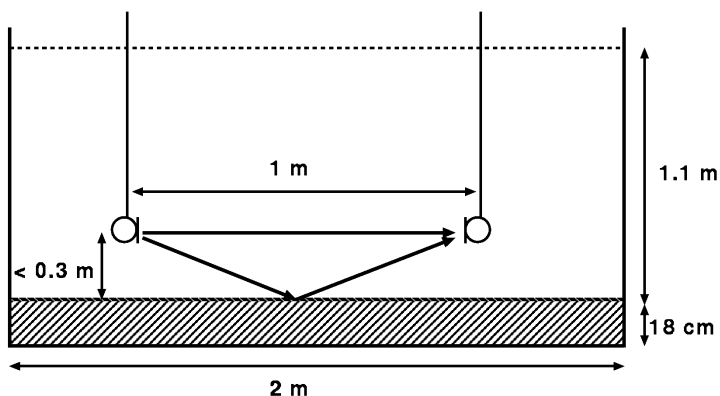
The standard sonar configuration with normal or close-to-normal sound incidence is not adequate for an acoustic detection of thin layers of undissolved fluid chemicals on the seafloor. This is due to the small impedance difference between the chemical and the water as well as the relative small layer thickness in comparison to the acoustic wavelength. For this reason the acoustic sensor is based on sound incidence at small grazing angles. In this technique the wave field above the seafloor consists of the directly transmitted and of the bottom reflected signal. The resulting interference pattern at the receiver location is then sensitively characterized by changes of the acoustic properties of the seafloor.

The technical realization of the grazing sound incidence is achieved by arrays of transmitters and receivers which are towed by the ROV close to the seafloor. The ROV also carries a hous-

ing which contains the electronic components for signal processing and controlling the position of the array elements.

2.2.1 Experimental setup

Scaled measurements were done in a water tank with a sand sediment layer on the ground. Two spherical hydrophones located in variable positions close to the ground were used. To prevent reflections from the tank walls and the water surface, chirp signals in the 2-200 kHz range with 0.5 ms duration were applied. Normalization of the acoustic transfer function between the hydrophones in the presence of the sediment to the spectrum of a formerly recorded free field measurement yields the excess attenuation function.



Sketch of the laboratory tank and the hydrophones positioned for measurements at grazing sound incidence. The grey area marks the sediment on the bottom of the tank.

2.2.2 Theory

The theoretical description of sound propagation above and in the sediment is based on the model of homogeneous stratified media. The influence of sediment properties as for example porosity is included in the Biot theory which predicts, in addition to the compressional wave in the water, a shear wave and two compressional waves in the sediment.⁸ Numerical modelling is done with the program FFLAGS (Fast Field Program for Layered Air Ground Systems).⁹ To solve the wave equation of a stratified medium consisting of homogeneous layers the inhomogeneous Helmholtz equation is written in cylinder coordinates:

$$\left[\nabla^2 + k_m^2(z) \right] \Psi_m(r, z) = S(\omega) \frac{\delta(r) \delta(z - z_s)}{2\pi},$$

where r denotes the radial distance from the source and z the height of the receiver above the ground. k_m is the wavenumber in the medium which is a function of the sound speed in the layer. The right side of the equation stands for the sound source with its frequency dependent source strength $S(\omega)$, positioned at height z_s and $r = 0$.

The Hankel transform of this equation with respect to the r -coordinate yields the following ordinary differential equation in z :

$$\left\{ d_z^2 - \left[k_r^2 - k_m^2(z) \right] \right\} \Psi_m(k_r, z) = \frac{f_s(z)}{2\pi} \quad \text{with} \quad \Psi(k_r, z) = \int_0^\infty \psi(r, z) J_0(k_r r, r) dr$$

J_0 is the Bessel function of the first kind to the order zero, and k_r is the radial wavenumber. The homogeneous solutions of this differential equation are easily evaluated. They correspond to plane waves in direction z :

$$\Psi_m(k_r, z) = e^{i\gamma z} \quad \text{with} \quad \gamma = \sqrt{k_m^2(z) - k_r^2},$$

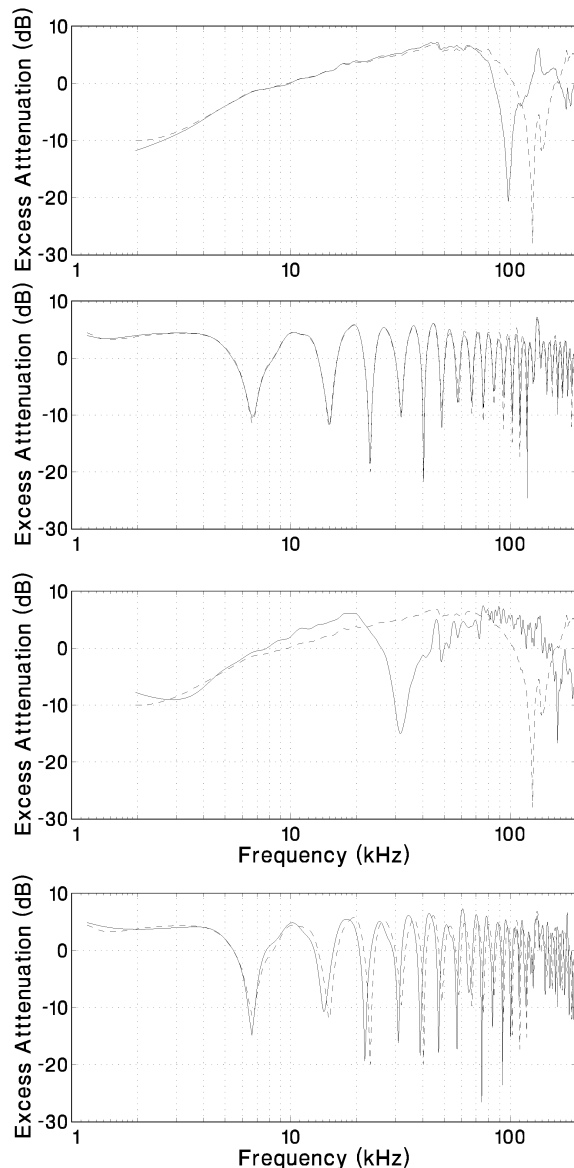
where the propagation constant γ still contains information about all layers. The general solution for a point source in a layer between z_1 and z_2 is:

$$\Psi_m(k_r, z) = \left\{ \frac{1}{\gamma} e^{-i|z_s - z|\gamma} + R_{\uparrow} e^{i(z_1 - z)\gamma} + R_{\downarrow} e^{i(z - z_2)\gamma} \right\}$$

The coefficients R_{\uparrow} and R_{\downarrow} follow from the boundary conditions for pressure and vertical particle velocity at the boundaries of adjacent layers. Other boundary conditions for the tangential and normal stresses and horizontal and vertical particle velocities in the skeleton hold for poroelastic layers. An inverse Hankel transform is required to translate this solution from k - to r space. In case of sufficiently large arguments $k_r r$ the Bessel function can be approximated by trigonometric functions. Then the inverse transform can be carried out using an ordinary Fourier transform for which efficient FFT algorithms are available.

2.2.3 Measurements and comparison with the theory

Measurements of the excess attenuation function above sand layers reveal that the presence of liquid chemicals causes a frequency shift of the interference pattern. This shift depends on the angle of the sound incidence, the acoustic impedance of the chemical, and its layer thickness. The figure given below shows data from layers of 1-Bromopentane with a sound velocity of 1042.8 m/s and a density of 1.22 g/cm³. The frequency shift of the dips increases with decreasing grazing angle and quantity of the liquid.

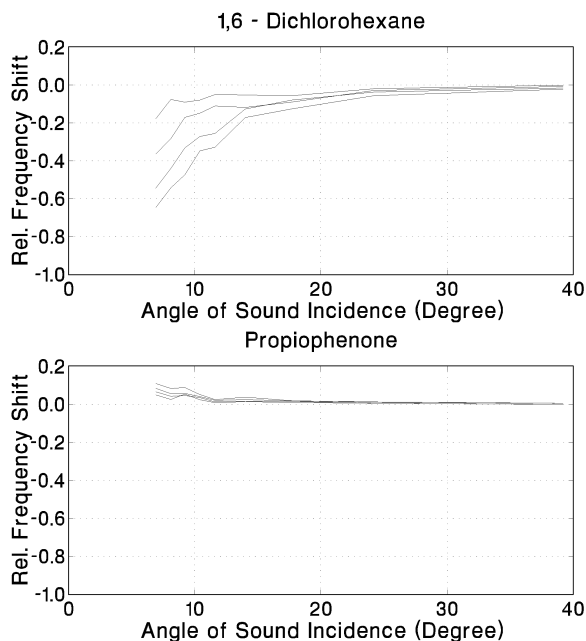


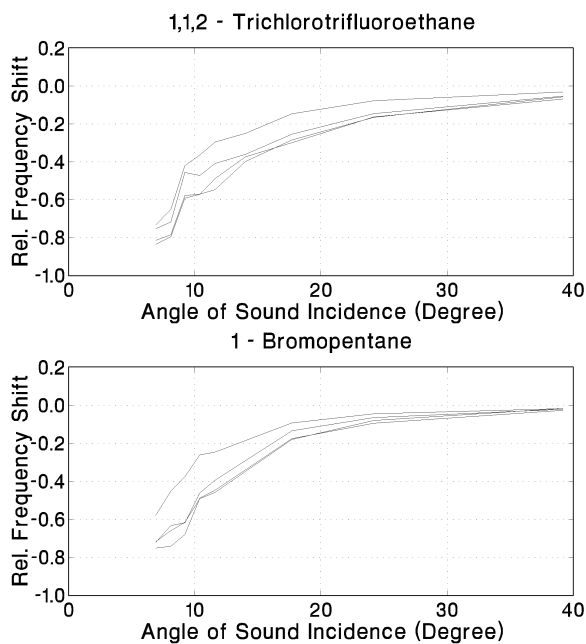
Excess attenuation measured over plain sand (dashed line) and sand covered with 1-Bromopentane (solid line) at 8.0 degree (left column) and 30 degree (right column) sound incidence. Film thickness is 0.1 mm (top) and 4.3 mm (bottom)

The relative frequency shift of the excess attenuation function caused by the poured substances was investigated systematically for various chemicals with different densities and sound speeds as a function of grazing angle, with the quantity of the chemical as the parameter. The interference pattern is shifted towards lower frequencies for chemicals with sound velocity lower than water. In case of higher sound velocity the pattern is shifted towards higher frequencies, as can be seen in the propiophenone measurement given below.

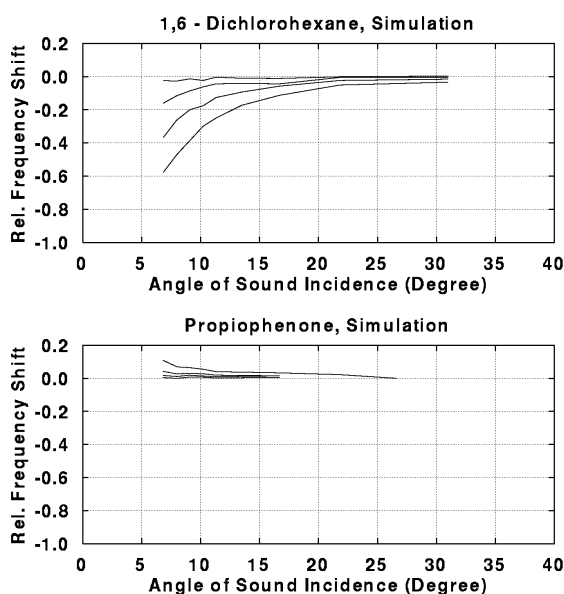
substance	sound velocity c [m/s]	density ρ [g/cm ³]	impedance $Z=\rho c$ [kg/m ² s]
bromopentane	1042.8	1.22	1272.2
1,3-dichlorobenzene	1259.3	1.29	1624.5
1,6-dichlorohexane	1327.5	1.07	1415.1
2,4-dichlorotoluene	1289.7	1.25	1612.2
propiophenone	1520.0	1.01	1535.2
1,1,2-trichlorotrifluoroethane	719.3	1.58	1136.6
water	1485.0	1.00	1485.0

Sound velocity, density and acoustic impedance of selected chemicals.





Measured relative frequency shift (i.e. frequency difference of the dips normalized to the frequency of the dips in the undisturbed interference pattern) as a function of grazing angle for various chemicals in quantities of 100, 500, 1000 and 2000 ml. These volumes correspond to an estimated film thickness of about 0.2, 2.2, 3.3, and 4.3 mm, respectively.



Simulation of the relative frequency shift of the dips in the excess attenuation function in the presence of a liquid chemical on the sediment. The layer thickness is set to values which correspond to the estimated thickness in the experiments given above.

The effect of the frequency shift and its measured dependence on angle and amount can be reproduced by numerical calculations as shown above. This agreement still holds for different types of chemicals.

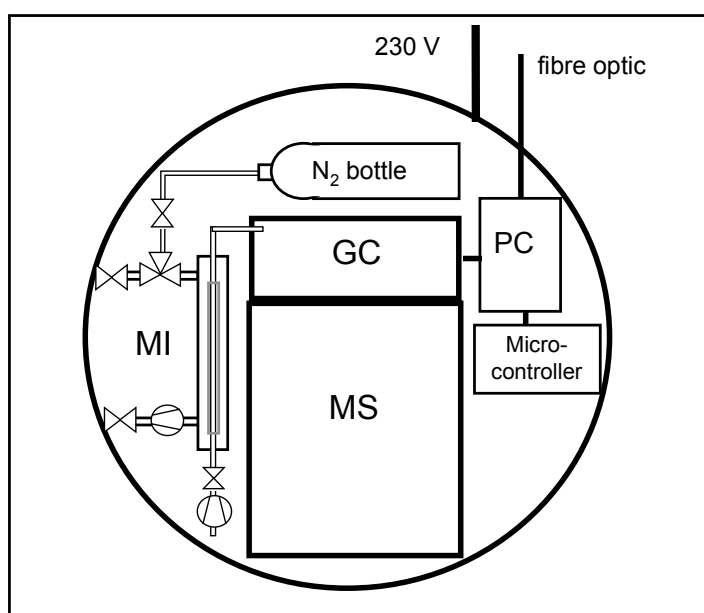
3 NEAR-FIELD SENSORS

3.1 The Membrane Induction/GC/MS system

A mass spectrometer as a multichannel detector provides evidence about the type and quantity of pollutants in water.¹⁰ Based on a mobile mass spectrometer (Model EM640, Bruker Franzen, Bremen) a submersible automated analysis system is under development. The sensor housing consists of high-strength, seawater resistant aluminum (AlMg4.5Mn). Its dimensions are L=1070 mm and D=640 mm, the mass is 158 kg.

3.1.1 Sampling principle

Membrane introduction mass spectrometry (MI/MS) has become a common sampling technique for the analysis of volatile organic compounds (VOC).^{11,12,13,14} For the coextraction of VOCs and semivolatile organic compounds (SOC) a heatable membrane probe has been developed. An extraction cycle starts with the sample step, in which an impeller pump sucks seawater through the membrane probe. VOCs permeate the membrane, whereas SOCs dissolve in the membrane material and are enriched.¹⁵



Components of the submersible MI/GC/MS

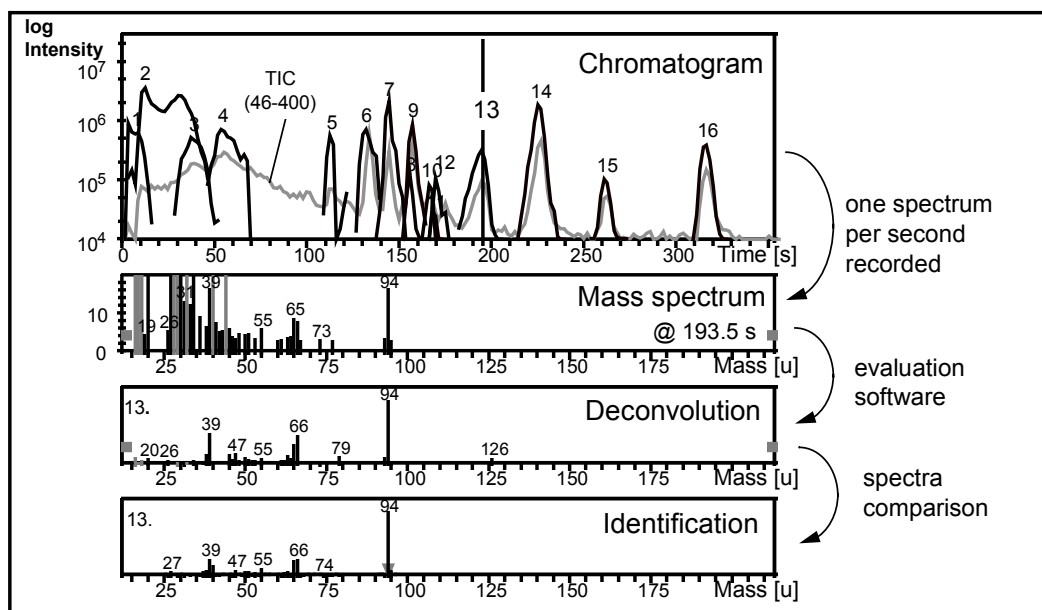
At the same time, a carrier gas stream through the membrane interior carries volatile compounds into the transfer capillary. At the end of the sampling step the water is removed from the tubing system with nitrogen gas. The blow out is verified with ultrasonic level instrumentation, and the pressure reducing valve is closed accordingly.

By heating the membrane probe the enriched SOCs are thermally desorbed, are flushed onto the gas chromatography column by the carrier gas and trapped at the head of the transfer capillary column. Seawater inflow cools the membrane within some seconds, and the next sample step is initiated.

Sampling, analysis and safety (i.e. sensors for humidity, temperature and pressure to protect the system from overheating and leakage) are controlled by a microcontroller (Philips 80C552). A logger provides a regular transfer of all measured values through a serial interface to a PC. This enables unrestricted access to measured data in real time.

3.1.2 GC/MS analysis

The high selectivity of the membrane separation process enables a rapid enrichment of organic compounds with simultaneous discrimination to the biogenic matrix. Since particles and dissolved compounds such as humic acid do not pervaporate, the separated sample can be transferred into the GC/MS without further sample preparation.¹⁶

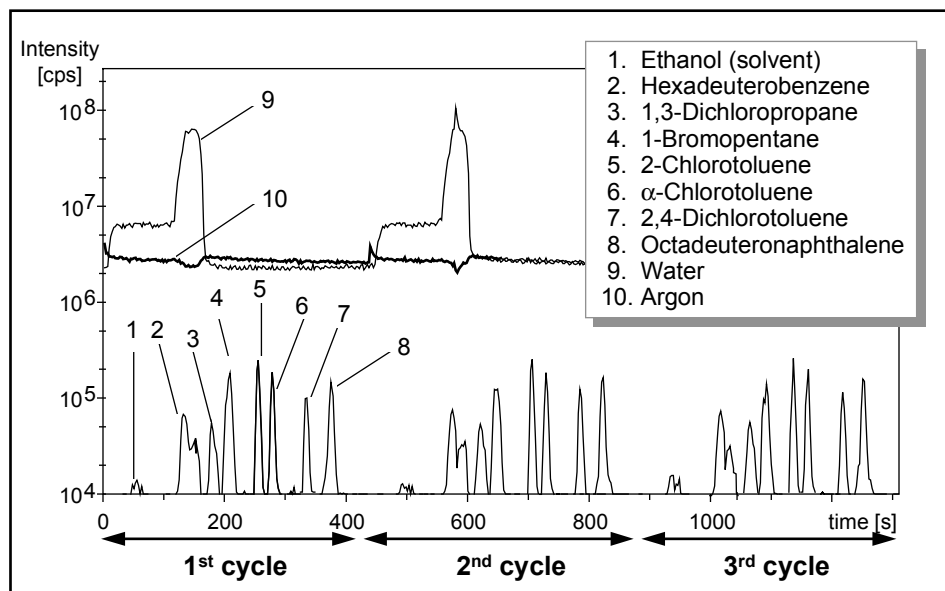


Automated evaluation of GC/MS data (Data Analysis, Bruker-Franzen, Bremen).

Rapid GC/MS analysis requires rapid separations by gas chromatography. This is achieved by the use of a short capillary column (6m) and a fast temperature program.^{17,18} Pollutant mixtures are separated into groups of similar evaporability.

The high compound specific mass spectra are separated by a deconvolution algorithm to derive pure compound spectra.¹⁹ Even without retention indices from HRGC a comparison with MS data bases is sufficient to identify most of the hazardous compounds.

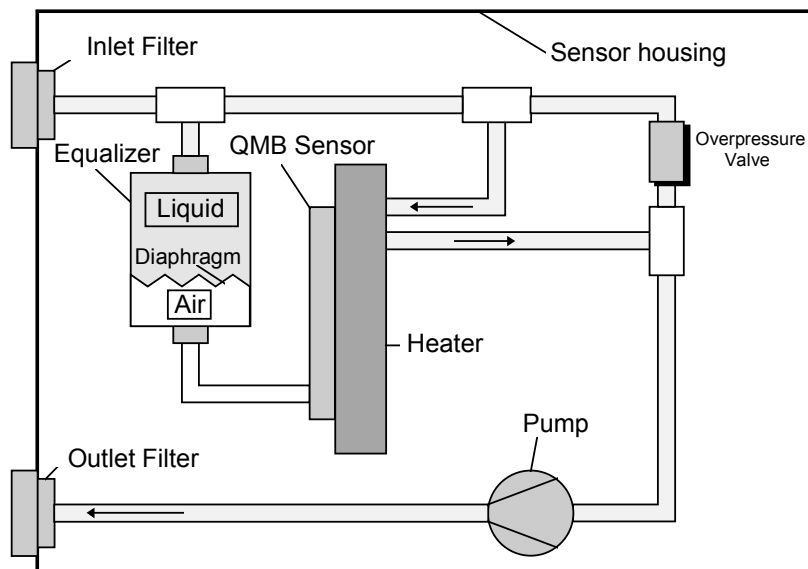
The chromatogram given above shows that a complete analysis cycle (enrichment, desorption, injection, chromatography, cleaning of the probe) is done in 7 minutes. The measured halogenated compounds possess small water solubility and higher density than water.



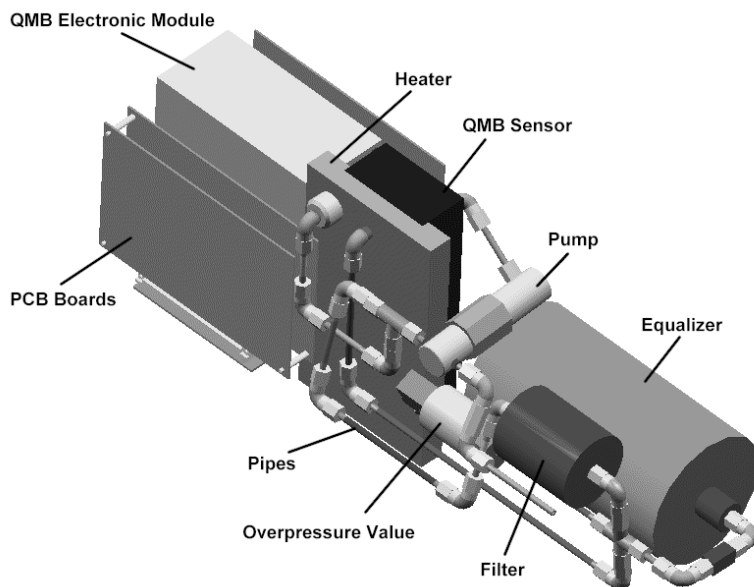
Three successive analyses (all concentrations: 50 µg/l, sampling time: 120 s)

3.2 The QMB sensor

The principle of the quartz crystal microbalance was first investigated by Sauerbrey in 1959. He described the relation between mass deposition on a quartz surface and the resulting change in the fundamental oscillation frequency of a quartz resonator in air.²⁰ Application of the quartz crystal as a chemical sensor requires a coating with sensitive and stable films.



Components of the quartz crystal microbalance (QMB) sensor

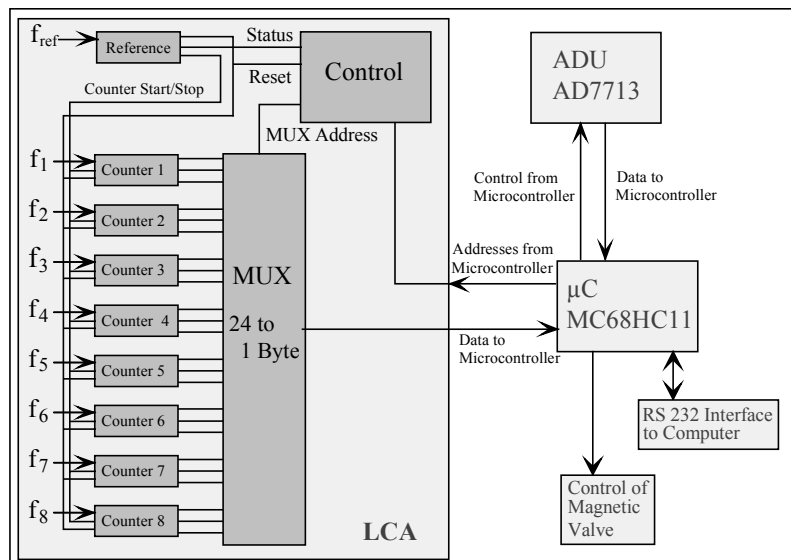


Mechanical configuration of the QMB sensor

The mechanical configuration inside the sensor housing is shown below. It has been designed for operation in seawater down to 300 m depth. A data acquisition and analysis tool processes and interprets the data. The software uses a neural network to identify specific chemical compounds.

The use of quartz crystal microbalance in liquids is critical since the viscous coupling between the liquid and the quartz surface, the surface roughness, possible surface stresses, changing liquid properties, and finally the driver electronics may also contribute to the observed frequency shift.^{21,22,23} Therefore, the sensor design has been optimized, including conditions in which the measurements are performed.

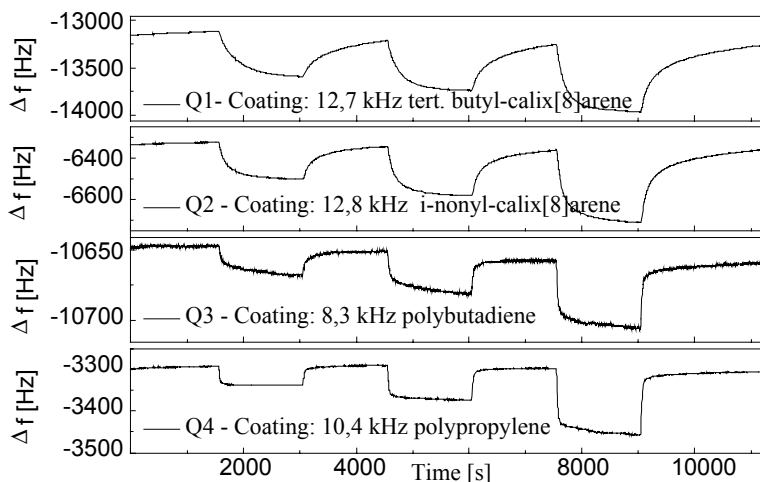
The measurement module has a compact structure and minimum hardware requirements. This is achieved by implementing SMD technology. The heart of the device is an LCA board with an LCA Model 4010D-84 (Xilinx). This device has an integrated serial port and programmable ROM. A microcontroller MC68HC11 is implemented to control the ADU and to read data from the LCA.



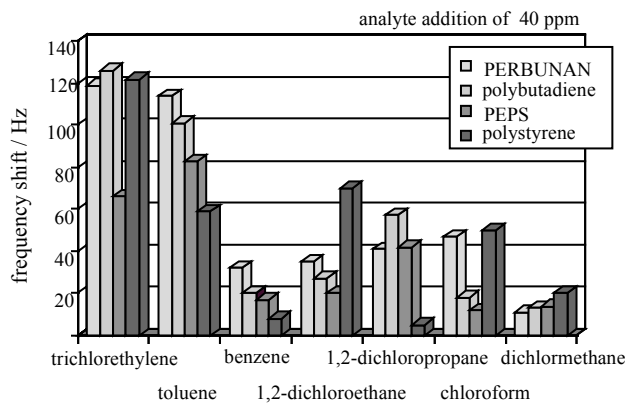
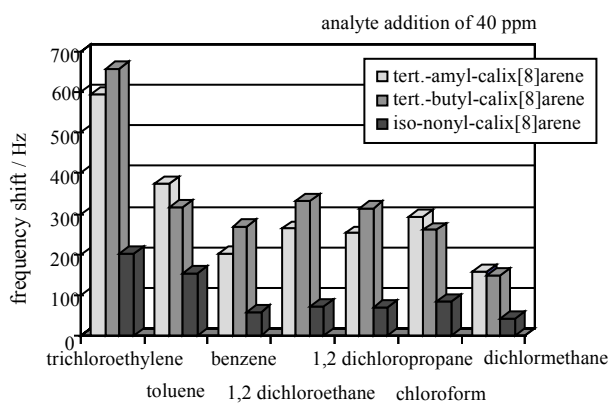
With the measurement module a parallel measurement of the resonant frequencies of eight quartzes and two temperature sensors is possible. Special attention has been paid to the design of the quartz oscillator²⁴ because of its high load which consists of the liquid and the viscoelastic load of the coating.

Schema of the measurement module

A measurement cell made of glass-ceramics has been developed which is equipped with eight quartz crystals. The quartzes are sealed with silicone glue. A very important factor is the sensitive coating of the quartzes. Therefore, various materials were tested and coatings such as the polymers polybutadien, polystyrene and polypropylene, and calix[8]arenes were chosen with best characteristics for the detection of organic pollutants.^{25,26}



Typical time response of QMB sensors coated with different layers. The negative frequency shift increases with analyte concentration (40, 80 and 160 ppm 1,2-Dichloropropane). After returning to pure water, the frequency returns to its baseline value.



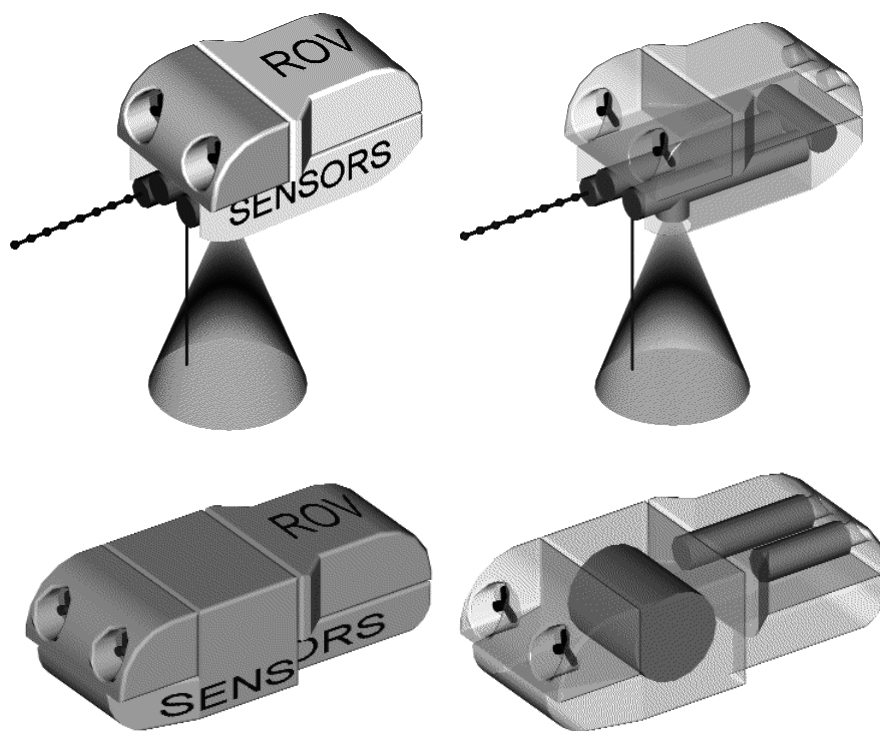
Signal pattern of different coatings to various analytes

The above figure illustrates the received signal pattern of various polymer and calix[8]arene coated QMB sensors from several analytes such as chlorinated and aromatic hydrocarbons. With these patterns and the use of neural networks or multivariate analysis it is possible to distinguish selected analytes.

4 SYSTEM PERFORMANCE

4.1 Sensor Platform

The operational platform of the sensor system is an ROV realised by MARISCOPE, Kiel, Germany. This ROV is specified for a maximum operation depth of 300 m with 3 knots maximum speed for the use in regions with high tidal currents. It is driven by up to 7 engines with a total power of 10.5 kW. Sensors are mounted in a frame of about 1,600 mm × 600 mm × 350 mm (L×W×H). The frame is fitted beneath the ROV engine unit. It is encased to ensure streamlined contours. Well positioned openings guarantee continuous water influx for *in situ* sensors and free field of view for the remote sensing instruments. An alternative frame of around 1,600 mm × 800 mm × 350 mm (L×W×H) is realized to carry larger instruments, e.g. the GC/MS.



ROV and sensor compartment, with laser beams for seafloor illumination and fluorescence analysis, and part of the towed array of the acoustic sensor. The QMB sensor is positioned in the front section of the payload frame.

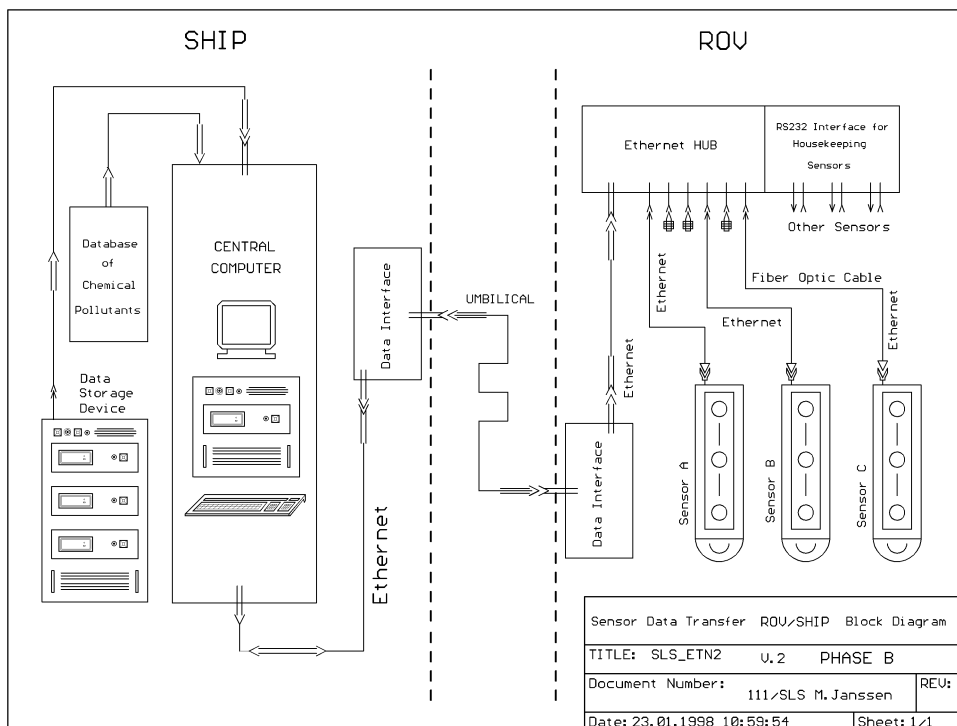
ROV equipped with a larger sensor compartment for using the MI/GC/MS, QMB and acoustic sensors.

4.2 Sensor Network

To enable a fast and efficient data interpretation, instruments and the control unit form an ethernet network. The central computer on board the ship is connected to the sensors in the payload frame of the ROV for instrument control and data acquisition. On the other hand, the central computer is connected to a data base of chemical pollutants and a mass storage device which allows for a joint data analysis and interpretation.

It is worth noting that a combined data acquisition and interpretation provides more information than a simultaneous operation of different instruments. Therefore, the system is handled like a single instrument. It forms an open frame structure with well-defined interfaces with the

perspective of an easy installation of other sensors in future, including an integration with other existing surveillance systems.



Schema of the ROV-based sensor network

5 ACKNOWLEDGMENTS

The authors express their gratefulness to the team members of their working groups who have made it possible to develop and realize this system for maritime pollution control: H. Harms, S. Harsdorf, M. Janssen, R. Matuschek, B. Wachowitz and R. Willkomm at the University of Oldenburg, R. Borngräber and Dr. S. Rösler at the University of Magdeburg, G. Kibelka at the Technical University of Hamburg-Harburg, H. Leonhardt at RST Rostock and many other colleagues in the mechanics and electronics workshops at these institutions. We also thank C. Haag and H. Schäfer from MARISCOPE, Kiel, for realizing the ROV.

Financial support of this joint project from the DLR Project Executive Department Environmental Protection and Technologies, Bonn, on behalf of the Federal Ministry for Research and Technology (BMBF), Germany, is gratefully acknowledged.

6 REFERENCES

- 1 Charles Simeonis: Analysis of existing information systems in the field of chemical pollution and their usefulness for the control of marine pollution. EC Commission, Final Report, Contract Number U/83/210, 1983.
- 2 Versuchsanstalt für Wasserbau und Schiffbau, Berlin, et al.: Bekämpfung sinkender und /oder gesunkener Chemikalien. Final Report, Federal Ministry for Research and Technology (BMBF), Germany, June 1992
- 3 J. Jaffe, The domains of underwater visibility, *Ocean Optics VIII, SPIE* Vol. 637, 287-293, (1986)
- 4 J.W. McLean and K.J. Voss, The point spread function in ocean water: comparison between theory and experiment, *Applied Optics*, 30, 2027-2030, 1991

- 5 F. Ahrenberg, S. Harsdorf, J. Niehues and R. Reuter, Contrast enhanced imaging in the sea: application of the optical transfer function for image reconstruction. In: *Proceedings of the 3rd EARSeL Workshop on Lidar Remote Sensing of Land and Sea*, Tallinn 1997, S. Babichenko and R. Reuter (editors). Published by EARSeL, Paris, in print
- 6 S. Harsdorf, M. Janssen, R. Reuter and B. Wachowicz, Submarine fluorescence lidar for environmental monitoring. In: *Proceedings of the 3rd EARSeL Workshop on Lidar Remote Sensing of Land and Sea*, Tallinn 1997, S. Babichenko and R. Reuter (editors). Published by EARSeL, Paris, in print
- 7 K.-H. Mittenzwey, G. Sinn, N. Roof and S. Harsdorf, An improved lidar method for monitoring surface waters: experiments in the laboratory, *Int. J. Remote Sensing*, Vol. 18, No. 11, 2271-2276, 1997
- 8 M. A. Biot, Generalized theory of acoustic propagation in porous dissipative media, *J. Acoust. Soc. Am.*, 34, 1254-1264, 1962
- 9 S. Tooms, S. Taherzadeh and K. Attenborough, Sound propagation in a refracting fluid above a layered fluid-saturated porous elastic material, *J. Acoust. Soc. Am.*, 93, 173-181, 1993
- 10 M.B Wise, C.V. Thompson, R. Merriweather and M.R Guerin, Review of direct MS analysis of environmental samples, *Field Analytical Chemistry and Technology*, 1, 251-276, 1997
- 11 T. Kotiaho, F.R. Lauritsen, T.K. Choudhury, R.G. Cooks and G.T. Tsao, Membrane introduction mass spectrometry, *Analytical Chemistry*, 63, 875A-883A, 1991
- 12 P.S.H. Wong, R.G. Cooks, M.E. Cisper, P.H. Hemberger, On-Line, In Situ Analysis with Membrane Introduction MS, *Environmental Science and Technology*, 5, 215-218, 1995
- 13 S. Bauer, Membrane introduction mass spectrometry: an old method that is gaining new interest through recent technological advances, *Trends in Analytical Chemistry*, 14, 202-213, 1995
- 14 N. Kasthurikrishnan, R.G. Cooks, On-line flow injection analysis of volatile organic compounds in seawater by membrane introduction mass spectrometry, *Talanta*, 42, 1325-1334, 1995
- 15 G. Matz and P. Kesners, Thermal membrane desorption application (TMDA) method for on-line analysis of organics in water by GC-MS, *Analisis*, 2, 12-16, 1995
- 16 G. Matz, F. Lennemann, On-line monitoring of biotechnological processes by gas chromatographic-mass spectrometric analysis of fermentation suspensions“, *Journal of Chromatography A*, 750, 141-149, 1996
- 17 G. Matz, W. Schröder, A. Harder, A. Schillings and P. Rechenbach, Fast on-site GC/MS analysis of hazardous compound emissions from fires and chemical accidents, *Field Analytical Chemistry and Technology*, 1, 181-194, 1997
- 18 G. Matz, W. Schröder, Fast GC/MS field screening for excavation and bioremediation of contaminated soil, *Field Analytical Chemistry and Technology*, 2, 77-85, 1996
- 19 P. Sander, Application of a fuzzy logic peak-finding algorithm for GC/MS Analysis, *Proceedings of the 43rd ASMS Conference on Mass Spectrometry and Allied Topics*, 724, 1995
- 20 G. Sauerbrey, Verwendung von Schwingquarzen zur Wägung dünner Schichten und zur Mikrowägung, *Z. Phys.*, 155, 206, 1959
- 21 J. Auge, P. Hauptmann, J. Hartmann, S. Rösler and R. Lucklum, New Design for QCM sensors in liquids, *Sensors and Actuators B*, 24-25, 43-48, 1995
- 22 J. Auge, P. Hauptmann, F. Eichelbaum and S. Rösler, Quartz crystal microbalance sensor in liquids, *Sensors and Actuators B*, 19, 518-22, 1994
- 23 J. Auge, J. Hartmann, P. Hauptmann and S. Rösler. Using Quartz-Crystal-Microbalance-principle for the detection and purity control of hydrocarbons in gases and as liquids, *Exp. Techn. Phys.* 40, 27-33, 1994
- 24 S. Rösler. Quarzresonator-Sensoren zum Nachweis chemischer Substanzen in Wasser. PhD thesis, University of Magdeburg, Germany, 1997
- 25 S. Rösler, R. Lucklum, R. Borngräber, J. Hartmann, P. Hauptmann, Sensor system for the detection of organic pollutants in water by thickness shear mode resonators, *Proceedings of Eurosensors XI*, Warszawa, Poland, 1997
- 26 J. Hartmann, J. Auge, R. Lucklum, S. Rösler, P. Hauptmann, B. Adler, E. Dalcanale, Supramolecular Interactions on mass sensitive sensors in gas phases and liquids, *Transducer '95*, Technical Digest, pp. 747-750, Eurosensors IX, Stockholm, Sweden, 1995